Surface Potential Characteristics of Polymeric Barriers for a Hybrid Gas-Solid Insulation

Surface Potential Characteristics of Polymeric Barriers for a Hybrid Gas-solid Insulation

Yuesheng Zheng, *Member, CSEE*, Qinfeng Liao, *Member, CSEE*, Bing Deng, *Member, CSEE*, Yilong Wang, *Member, CSEE*, and Yuriy V. Serdyuk

***Abstract*—The effect of barrier material on AC breakdown voltages of a hybrid gas-solid insulation is investigated by examining the behavior of electrostatic potential on barrier surfaces. Breakdown characteristics of air-insulated gaps with barriers made of three different polymeric materials are experimentally investigated. Further, measurements of surface potential on the barriers are performed and the results are utilized to obtain surface charge dynamic characteristics for the three polymeric materials and extract their electric conductivities, charge carrier mobilities, and trap energy distributions. It is found that the material with the lowest initial surface potential and fastest decay rate exhibits the highest bulk conductivity and carriers' mobility, as well as the lowest trap energy level. These properties provide the highest increase in AC breakdown voltages compared with pure air. It is concluded that materials where the accumulation of charges in the bulk is inhibited and decay of surface charges is facilitated, allow for higher operating voltages of AC hybrid gas-solid insulation systems. The mechanism of the effect of barrier material on AC breakdown voltage is discussed.**

***Index Terms*—Bulk conductivity, carrier mobility, hybrid insulation, surface potential decay, trap density.**

I. Introduction

AIR is widely used as an insulating gas in medium-voltage electrical equipment at rated voltages below 12 kV (for devices manufactured in China). In contrast, sulfur hexafluoride (SF_6) is commonly employed at higher voltages [1], [2]. The use of SF_6, which is a gas with extremely high global warming potential, is to be restricted in the future due to environmental concerns, and thus, new solutions need to be found to provide comparable electrical strength of the insulation. Ideally, SF_6 is to be substituted by air. However, the withstand voltage of the latter is approximately three times lower. Hence, its performance should be enhanced, and one of the promising ways is to introduce solid insulating barriers at suitable locations in air gaps between energized electrodes. Earlier performed studies have demonstrated that a positive effect of a barrier can be achieved under AC, DC, and impulse voltages [3]–[5]. However, its efficiency is affected by several factors. Breakdown voltages are found to be increasing with increasing barrier size [6]. However, its optimal position between electrodes depends upon electric field distribution. Furthermore, since charges will accumulate on gas-solid interfaces, one may expect the performance of such hybrid systems to be affected by the material of the barrier. However, publications on this subject are rare (see e.g. [7]), and no systematic studies have been reported so far. This has led to the situation that there are no recommendations for criteria for choosing barrier material for higher breakdown voltage of hybrid air-solid insulation systems.

Charging of a solid barrier is caused by pre-breakdown discharges in the surrounding gas, which may appear at voltages below the breakdown threshold and generate charged species [8]–[10]. Being driven by the electric field, these charge carriers will accumulate on gas-solid interfaces [11]. In the rod-plate insulation gap, charges on the barrier surface will weaken the electric field intensity near the rod electrode, thereby inhibiting the inception of the streamer and increasing breakdown voltage [12]. In addition, charges accumulated on the gas-solid interface will influence the breakdown path [13]. However, charges accumulated on the basin insulator in gas-insulated switchgear and gas-insulated transmission lines will distort electric field distribution in air and increase the maximum value of the electric field near the high voltage electrode [14], [15]. Under impulse voltage, charges accumulated on the surface of the barrier will cause a restrike in the gaps [16]. Therefore, the dynamics of surface charges are important for the barrier effect.

One of the ways to investigate charge dynamic characteristics is by utilizing surface potential measurements. In such experiments, the potential of the material surface is monitored after charging with DC corona, electron beam, or impulse voltages [17], [18]. As surface charge density has a direct relationship with the surface potential, variation of the latter can reflect the dynamics of charges [20], [21]. According to the results of surface potential decay (SPD) measurements, it was observed that the polarity of charging may lead to different charge (potential) distributions on solid dielectric surfaces [22]. SPD rates are also affected by surrounding air conditions (e.g., increased humidity [23]). It has been shown

Manuscript received September 29, 2021; revised December 25, 2021; accepted January 4, 2022. Date of online publication October 12, 2022; date of current version April 4, 2025. This work was partly supported by the National Natural Science Foundation of China (51607041) and China State Key Lab of Power Systems (SKLD19KM06).

Y. S. Zheng (ORCID: https://orcid.org/0000-0002-4498-8001), Q. F. Liao, B. Deng and Y. L. Wang (corresponding author, email: 1091494402@qq.com, ORCID: https://orcid.org/0000-0002-2274-1032) are with Fujian Province Key Laboratory of New Energy Generation and Power Conversion, the College of Electrical Engineering and Automation, Fuzhou University, Fuzhou 350108, China.

Y. V. Serdyuk (ORCID: https://orcid.org/0000-0003-1803-2660) is with Department of Electrical Engineering, Chalmers University of Technology, Gothenburg SE-412 96, Sweden.

DOI: 10.17775/CSEEJPES.2021.07330

that SPD rate depends on different materials under similar conditions, and this fact was used for deriving various material characteristics, such as field-dependent volume conductivity and trap energy distribution [24]–[27]. It should be noted, however, that SPD studies focused mainly on basic materials characterization rather than on particular applications, such as choices of materials for higher insulation performance and methods for manufacturing samples. Thus, thin films of polymers (polyethylene, polypropylene, etc.) and samples of millimetre thickness of silicone rubbers and epoxy resins were utilized in most investigations without considering mechanical stiffness and resistance to arcing, which are important for securing a reasonable lifetime of insulating barriers.

In the present paper, the behaviour of surface potentials on pre-charged samples of three polymeric materials used in a hybrid gas-solid insulating system is investigated. Their bulk conductivities, carrier mobility, and trap energy distributions are derived from respective SPD characteristics. Besides, measured AC breakdown voltage characteristics of hybrid gas-solid insulation systems with barriers made of these three materials are presented and discussed.

II. Experimental Setup

A. Surface Potential Measurement

A surface potential measurement system is shown in Fig. 1. Surface potential of the barrier was measured using a Kelvin probe mounted on the same arm and kept at 2 mm above the sample surface. The probe was connected to a Trek347 high-voltage amplifier. Measured surface potential was recorded utilizing data acquisition card USB-6211 (from NI). Air conditions were recorded by a data logger TR-73U. The sample was exposed to corona discharge from a needle (0.79 mm in diameter). The needle was fixed 36 mm above the center of the sample surface. A charging DC voltage of 6 kV was applied to the needle. Materials used in the study were epoxy resin/glass composite (FR4), polymethyl methacrylate (PMMA), and polyvinyl chloride (PVC). Dimension of the sample was 120 mm × 120 mm × 3 mm. Before the experiment, the sample was cleaned with absolute alcohol and dried in air for 12 hours. An ionization blower was used to eliminate the residual charge on the sample before the next charging. An initial scan of the potential on the sample surface was performed to check the charge-free state.

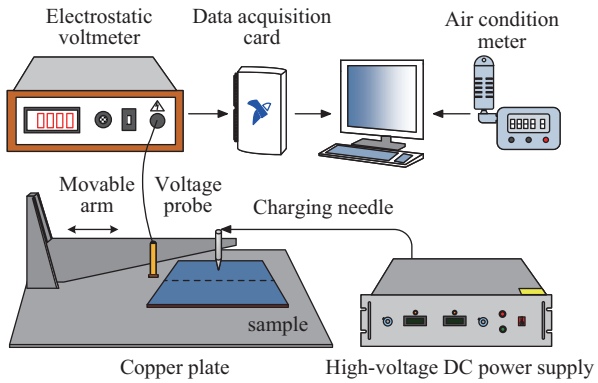

Fig. 1. Schematic of surface potential measurement system.

In the initial potential experiment, charging time was set at 1 minute, 2 minutes, 5 minutes, and 10 minutes, respectively. After corona charging, the probe was moved to the center of the sample to measure the initial potential. In the surface potential decay experiment, the charging time was 5 min, and the applied voltage was 6 kV. After corona charging, the potentials on the barrier along the scan line were measured. Due to the symmetry of the surface potential distribution, the scan was performed on half the scan line to shorten the scan time and to improve the accuracy of the measurement [28]. After the scan, the probe was moved to the center of the sample to obtain the SPD characteristics. The SPD measurement process lasted up to 10 hours. The following air conditions were recorded during the initial surface potential measurements: temperature 32±1°C, relative humidity 44±2%RH, and pressure 1012±1 hPa.

B. Breakdown Voltage Test

The experimental setup used for breakdown tests is shown in Fig. 2. Effect of the barriers was analyzed using a rod-plane electrode system. Radius of the rod tip r was 0.5 cm and distance between the electrodes d was 5 cm. Position a of the barrier was varied in the experiments from 1 cm to 4 cm with a step of 1 cm as accounted from the tip of the rod. The rod electrode was connected to the transformer, providing voltages of up to 100 kV_{rms} at 50 Hz through a protective resistor. The plane electrode was grounded. Test voltage was measured by a voltage divider. Before experiments, the barrier and the electrodes were cleaned with absolute alcohol. The applied voltage was increased at a RSM rate of 2 kV/s until breakdown. Every sample was tested 20 times and 1 minute resting time was applied between consecutive experiments. The air conditions during the experiments were: temperature 27.9±1.8°C relative humidity 78±5%RH, and pressure 1008 ±3 hPa.

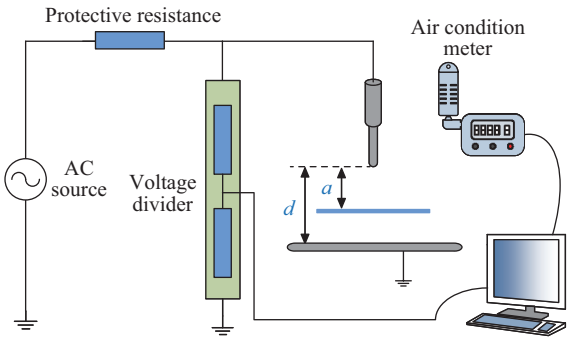

Fig. 2. Schematic of breakdown voltage test system.

III. Surface Potentials Characteristics

A. Initial Surface Potential

The initial surface potentials of different materials at different charging times are shown in Fig. 3. The surface potential of FR4 is always the lowest among the three materials at different charging times. The surface potential of FR4 is the lowest among the three materials. The initial surface potential of FR4 at 1 min is 2.09 kV. It increases from 2.09 kV to

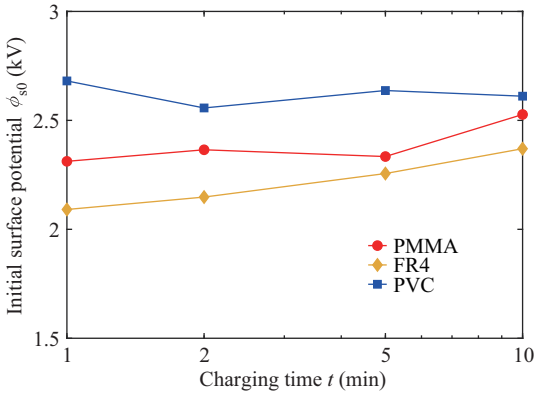

Fig. 3. Initial surface potentials on different materials at different charging times.

2.37 kV as the charging time increases from 1 min to 10 min. When the charging time is shorter than 5 min, the initial potential of PMMA is about 2.34 kV. When the charging time is extended to 10 min, the initial potential of PMMA increases to 2.53 kV. The initial surface potential of PVC is 2.68 kV at 1 min. And the surface potential of PVC is around 2.6 kV with increasing the charging time. Surface potentials of FR4 and PMMA increase with increasing charging time when charging time is shorter than 10 min. It indicated that the surface charge decay rates of FR4 and PMMA are slower than those of the surface charge accumulation rate.

B. Surface Potential Decay

Surface potential distributions measured at different times after charging on different materials are shown in Fig. 4. One may notice that surface potential profiles on the barrier are bell-shaped. Surface potentials are highest at the center of the samples (coordinate $x = 0$ cm), where the corona needle was located during charging. It can be seen that surface potential decreases with time. After a decay time of 50 min, the surface potential at the center of FR4 barrier is about 0.71 kV, whereas the potential on PMMA barrier is reduced to 1.82 kV. However, the decay of surface potential in the center of PVC barrier is not obvious. The SPD rate is higher for FR4 than for PMMA and PVC.

The SPD rates are quantified in Fig. 5, where normalized surface potential decay characteristics obtained for different materials are presented. Note that data shown in Fig. 5 were measured at the centers of the samples, and the first measurement was taken almost immediately (at about 1 s) after completing the charging stage. As can be seen, characteristics reveal that SPD is fastest on FR4, as also observed in surface potential distributions in Fig. 4. Thus, the time to decay to half of the initial surface potential value is about 10^3 s, which is one order of magnitude shorter than the respective time for PMMA. As for PVC, the decay is much slower, and, at the longest measurement time 5×10^4 s, the potential reduced just to about 90% of its initial magnitude.

IV. Materials Properties Derived From SPD

A. Bulk Conductivities

Three physical processes are usually adopted to explain the

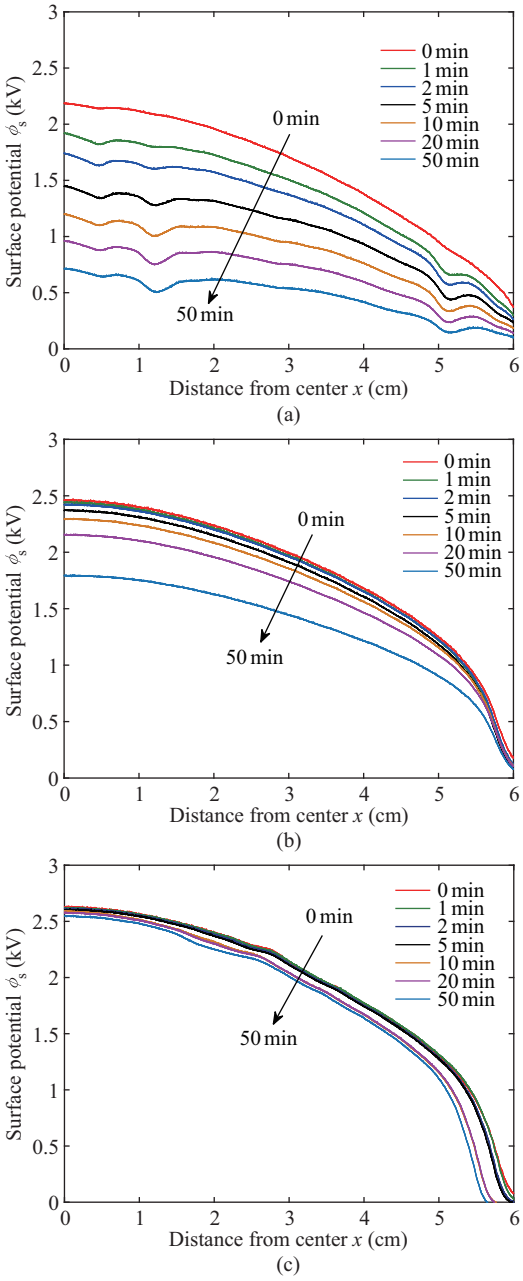

Fig. 4. Surface potential distributions at different times after charging on samples of (a) FR4, (b) PMMA and (c) PVC.

reduction of the amount of deposited surface charges with time, namely, surface conduction, bulk conduction, and charge neutralization by gas ions [29]. As mentioned above in relation to Fig. 4, surface conduction does not play any significant role under the conditions of the present study. Also, the specific feature of the potential probe used prevents the accumulation of air ions, which may neutralize deposited charges. Therefore, the decay process can be assumed to be solely controlled by bulk conduction mechanisms in the materials stimulated by the electric fields induced by deposited surface charges. Accounting for this and noting that the material sample is in open circuit conditions during the surface potential decay process, the sum of the displacement and conduction currents in the material is

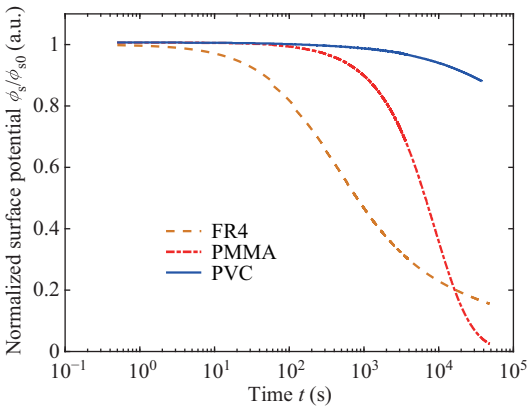

Fig. 5. Normalized surface potential decay measured on different materials.

$$\varepsilon\frac{\partial E(x,t)}{\partial t}+\sigma E(x,t)=0 \tag{1}$$

where E stands for the electric field in the sample, V/m; σ is the bulk conductivity, S/m; ε is the permittivity of the material, F/m; x is the coordinate accounted from sample's surface, m; and t is the elapsed time after charging, s. Assuming the electric field in material is uniform $E=\phi_s/L$ (here, ϕ_s is the surface potential, V, and L is sample thickness, m), one can obtain the expression for the material conductivity as written by:

$$\sigma(\phi_{\rm s})=-\frac{\varepsilon}{\phi_{\rm s}(t)}\frac{{\rm d}\phi_{\rm s}(t)}{{\rm d}t} \tag{2}$$

Equation (2) results in exponential type of surface potential decay:

$$\phi_{\rm s}(t)=\phi_{\rm s0}e^{-\frac{\sigma}{\varepsilon}t} \tag{3}$$

where $\phi_{\rm s0}$ is the initial magnitude of the surface potential (right after charging). From (3), it can be observed that surface potential decay rate is related to time coefficient τ, which can be defined as:

$$\tau(t)=-\frac{1}{t}\ln\frac{\phi_{\rm s}(t)}{\phi_{\rm s0}} \tag{4}$$

In the present study, relative permittivities of the materials were experimentally measured by the IDAX300 insulation diagnostic analyzer. A three-electrode measurement system was used in the experiment [30]. The diameters of center electrode, ring electrode, and top electrode are 50.8 mm, 57.2 mm, and 85.7 mm, respectively. The applied voltage had a RSM value of 140 $V_{\rm rms}$ with a frequency range from 0.01 Hz to 1000 Hz. Measured relative permittivities of the materials at 100 Hz are given in Table I.

Based on the data in Table I, time coefficients were calculated using (4), and results are shown in Fig. 6. It can be observed that coefficients τ obtained for different materials decrease with time. Magnitudes are highest for FR4 during significant time intervals after charging but decrease rapidly. In contrast, the time coefficient of PMMA is much lower but is almost constant after initial essential reduction. The time coefficient of PVC is smallest compared to other materials and shows a decreasing trend similar to FR4.

TABLE I
RELATIVE PERMITTIVITIES OF THE MATERIALS

Material	FR4	PMMA	PVC
Relative permittity@100Hz	6.2	4.3	3.1

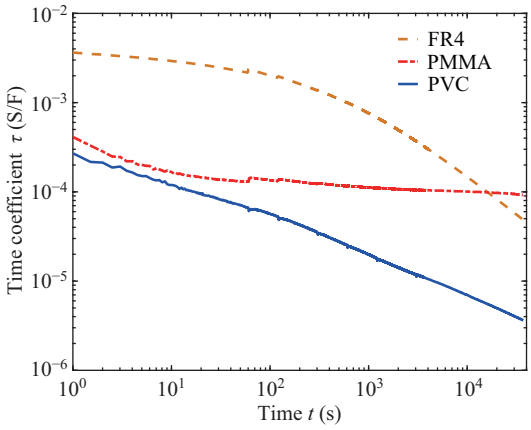

Fig. 6. Surface potential decay time coefficients of different materials.

Besides, according to (3), the dependence of the material conductivity on surface potential and time can be obtained as:

$$\sigma(t)=-\frac{\varepsilon}{t}\ln\frac{\phi_{\rm s}(t)}{\phi_{\rm s0}} \tag{5}$$

Conductivities calculated using (5) with the relative permittivities of the materials given in Table I and measured SPD characteristics in Fig. 5 are shown in Fig. 7. It can be observed that bulk conductivities of the tested materials are higher at the beginning of the potential decay and decrease with time. Comparing their magnitudes for different materials, one may notice that the conductivity of FR4 is highest most of the time in the measured interval. The conductivity of PMMA is rather constant and is lower than that of FR4. PVC is the most resistant material among those used in the present study. Taking into account that surface potential decays with time, the electric field in the material is decreased. Results in Fig. 7 indicate the bulk conductivities of the materials are field-dependent.

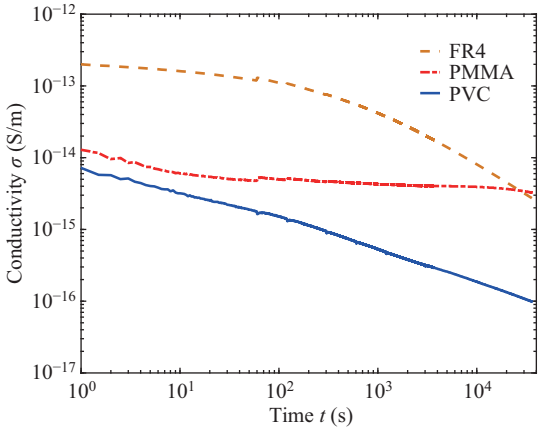

Fig. 7. Bulk conductivities of different materials.

B. Charge Carriers Mobility

Carrier mobility is an important parameter that describes the average velocity of motion of charges in the material under the electric field. Charge mobility plays a critical role in the DC breakdown mechanism of XLPE [31]. Therefore, carrier mobility may also affect the breakdown voltage of hybrid gas-solid insulation. In this study, carrier mobility μ is derived from the SPD measurements and is given by [32]:

$$\mu = \frac{L^2}{t_T \phi_{s0}} \tag{6}$$

where L is the thickness of the sample, t_{T} is the transit time at which the implanted charge migrates to the grounded electrode. The latter can be estimated by considering the dependence of surface potential decay rate $\lg(|\mathrm{d}\phi/\mathrm{d}t|)$ with respect to t [33], which is schematically shown in Fig. 8. One may notice the lines approximating the behavior of $\lg(|\mathrm{d}\phi/\mathrm{d}t|)$ on the initial and final stages of the decay process intersect at the time instant which can be approximately taken as the transit time t_{T}.

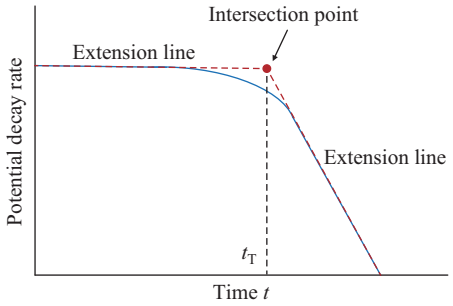

Fig. 8. Schematic diagram of the corner point t_{T}.

By applying this approach to measured SPD characteristics, transit times and charge carrier mobilities were derived for the studied materials, and results are shown in Table II. As can be observed, the highest mobility values are obtained for FR4, and PVC is characterized by the lowest carrier mobility. This indicates that charges deposited on the surface of FR4 migrate to the ground electrode within a relatively short time. As a result, the surface potential decay rate on FR4 is faster than that of PMMA and PVC.

TABLE II
CORNER POINT AND CARRIER MOBILITY OF DIFFERENT MATERIALS

Material	FR4	PMMA	PVC
Knee point time (s)	9.51×10^5	1.689×10^6	2.308×10^6
Carrier mobility ($m^2/(V \cdot s)$)	4.3377×10^{-15}	2.1668×10^{-15}	1.4847×10^{-15}

C. Trap Energy Distribution

Transport of electric charges through the material is associated with its trapping and de-trapping. Assuming that charge carriers released from traps are not trapped again immediately, and that surface potential decay takes place under isothermal conditions, distribution of the trap energy can be obtained as [20], [21]:

$$N(\Delta E) = \frac{4\varepsilon_0 \varepsilon_{\mathrm{r}}}{qkTL^2} \left| t \frac{\mathrm{d}\phi_{\mathrm{s}}}{\mathrm{d}t} \right| \tag{7}$$

where N is trap density at energy level E, $\mathrm{eV}^{-1}\mathrm{m}^{-3}$; ε_0 is the permittivity of vacuum, F/m; ε_r is the relative permittivity of the material; q is the elementary charge, C; k is the Boltzmann's constant, J/K; T is the absolute temperature, K. Trap energy level ΔE can be derived from demarcation energy theory as where ν is the attempt to escape frequency, s^{-1}, which is set to 6.2×10^{12} s^{-1} [34] in the present study.

$$\Delta E = kT \ln(\nu t) \tag{8}$$

Trap energy distributions obtained for the studied materials are shown in Fig. 9. As seen, the maximum trap density appears at about 0.96 eV in FR4 and at about 1 eV in PMMA. Although the trap density peak of PVC is not seen in Fig. 9 due to limited measuring time, they can be expected at higher energy levels. Besides, the trap density for FR4 is highest, and PMMA is second, while the density level of PVC is much lower. One should note that shallower traps (lower energies) indicate easier de-trapping of charge carriers and, thus, faster decay, which is consistent with the measured SPD characteristics.

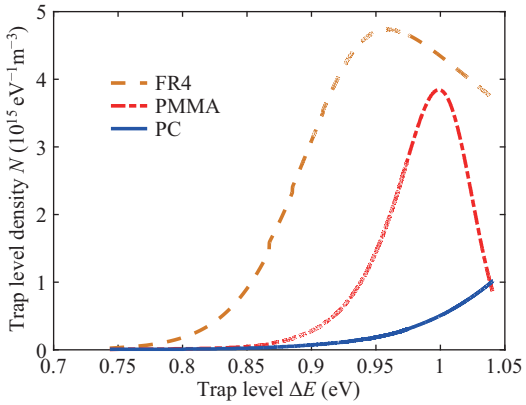

Fig. 9. Trap density distributions derived for different materials.

V. BREAKDOWN VOLTAGE

Normalized breakdown voltages (i.e., the ratio of breakdown voltage measured with a barrier to that of pure air $U_{\mathrm{b}}/U_{\mathrm{b0}}$) of the hybrid gas-solid insulation obtained with different barrier materials are shown in Fig. 10. As can be observed, the presence of solid barriers leads to an increase of breakdown voltages and the effect is more significant when the barrier is positioned closer to the rod electrode. In the latter case, enhancement of the insulation performance reaches about 90% compared to pure air when barriers made of PMMA and PVC are used. FR4 provides the essential increase of breakdown voltages, which is observed when the barrier was located close to the rod electrode at $a/d = 0.2$ and 0.4. Observed variations of breakdown voltages can be correlated with the dynamic behavior of charges on the barrier surface. Thus, when the applied voltage induces the electric field at

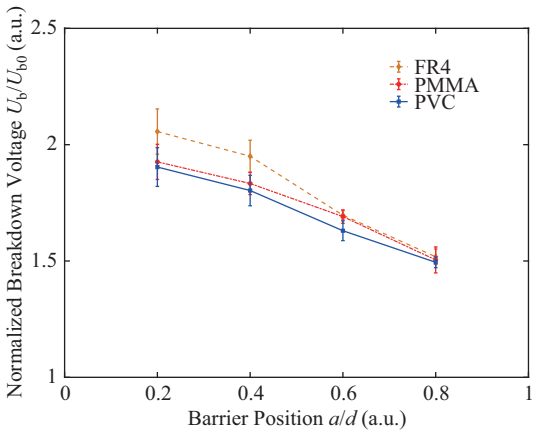

Fig. 10. Normalized breakdown voltages obtained with different barrier materials at different positions in gas gap.

the tip of the rod electrode strongly enough to initiate pre-breakdown discharges, generated charge carriers will drift in the field and accumulate on the barrier. These charges may produce their own field, which is superimposed on the applied field. As a result, the electric field between the rod electrode and the barrier is weakened if the surface charge is of the same polarity as the potential of the rod electrode [35]. When the polarity of the applied voltage reverses, the electric field in the gap between the rod electrode and barrier can be significantly strengthened if the accumulated surface charges remain unchanged, which may provide conditions for breakdown. However, if the material of the barrier is characterized by weak charge trapping capability and charge decay of its surface is fast enough, field strength may not reach the breakdown threshold at polarity reversal, and thus, higher breakdown voltages can be achieved. This may be the case for FR4 materials in the present study, which demonstrate the fastest SPD (Fig. 5) and most shallow traps (Fig. 9) and, respectively, provide the highest breakdown voltages (Fig. 10) among the studied materials.

VI. Discussion

According to the previous experimental results, the effect of materials on breakdown voltage is significant when barriers are close to the rod electrode. During the experiment, breakdown paths were photographed and statistically analyzed. Breakdown paths are divided into two types, as shown in Fig. 11. Thus, Fig. 11(a) shows path Type I, which indicates discharge development along the barrier surface to the ground electrode. Fig. 11(b) depicts path Type II, where discharge progresses directly to the barrier edge and then reaches the grounded electrode. It was observed in the experiments that when the barrier was close to the rod electrode, the probability of occurrence of path Type I was much higher than of path Type II in 20 consecutive breakdowns. When the barrier is far away from the rod electrode, the occurrence probability of path Type II exceeds that of path Type I. These results are consistent with all barrier materials used.

Furthermore, it can be expected that breakdown voltage is affected by the barrier material when path Type I occurs,

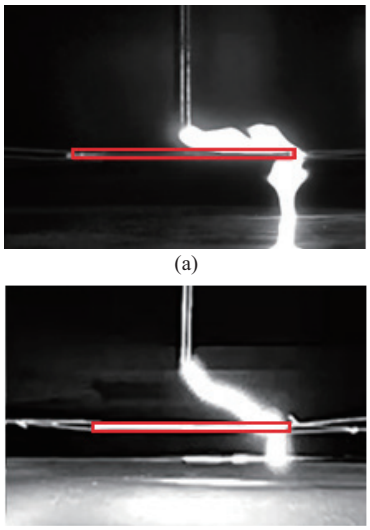

(a)

(b)

Fig. 11. Breakdown paths at different barrier positions. (a) Path Type I. (b) Path Type II.

whereas it has no relationship with barrier material when path Type II occurs. This can be explained by conditions on the barrier surface. Thus, when the barrier is close to the rod electrode and path Type I occurs, a part of the breakdown path is on the barrier surface. Under this condition, the breakdown voltage is affected by the barrier material due to different charge behaviors on the barrier surface, specifically, its conductivity, charge carriers' mobility, and energy of traps. Hence, when a barrier is introduced into an air gap at the position of $a/d < 0.5$, a barrier made of material providing a higher SPD rate provides efficient enhancement of the breakdown voltage. At the same time, for a barrier placed at the position of $a/d > 0.5$, the effect of its material on breakdown voltage is insignificant. Then, high voltage tests of the withstand voltage can be reduced, which can provide a reference for the insulation design of the gas-solid hybrid insulation.

VII. Conclusion

Surface potential characteristics of PVC, PMMA, and FR4 materials were investigated. The initial surface potential of PVC was found to be the highest, whereas it was lowest on FR4. In addition, the fastest surface potential decay was observed on FR4. Bulk conductivities, charge carrier mobility, and trap energy distribution were calculated based on surface potential characteristics. The highest bulk conductivity and carrier mobility were found on FR4 and the lowest on PVC. Moreover, FR4 was characterized by the lowest level of trap energy density, followed by PMMA and PVC. As for the effect of barrier position, the strongest influence of the barrier on breakdown voltages was observed when the barrier was closer to the rod electrode. The most significant increase in the breakdown voltages was provided by the barrier made of FR4, which allows us to conclude that under the same charging conditions, the material with the lowest initial surface potential and the fastest decay rate ensures the best performance of AC hybrid insulation systems.

REFERENCES

[1] J. R. Wang, Q. M. Li, H. Liu, W. Jian, Y. A. Chang, Q. Hu, and M. A. Haddad, "Impact of SF_6 decomposition products on epoxy resin chemical stability and doping-nano-Al_2O_3-based enhancement using the ReaxFF-MD method," *CSEE Journal of Power and Energy Systems*, vol. 9, no. 2, pp. 779–789, Mar. 2023.

[2] H. Y. Zhou, G. M. Ma, M. Zhang, C. Wang, Y. P. Tu, and C. G. Li, "Insulation design rule for a spacer in SF_6/N_2-filled DC gas insulated apparatus," *CSEE Journal of Power and Energy Systems*, vol. 10, no. 2, pp. 727–735, Mar. 2024.

[3] H. K. Meyer, F. Mauseth, A. Pedersen, and J. Ekeberg, "Breakdown mechanisms of rod-plane air gaps with a dielectric barrier subject to lightning impulse stress," *IEEE Transactions on Dielectrics and Electrical Insulation*, vol. 25, no. 3, pp. 1121–1127, Jun. 2018.

[4] Y. Chen, Y. S. Zheng, and X. R. Miao, "Breakdown conditions of short air-insulated gaps under alternating non-uniform electric fields," *Journal of Applied Physics*, vol. 122, no. 3, pp. 033304, Jul. 2017.

[5] E. Foruzan, A. A. S. Akmal, K. Niayesh, J. Lin, and D. D. Sharma, "Comparative study on various dielectric barriers and their effect on breakdown voltage," *High Voltage*, vol. 3, no. 1, pp. 51–59, Oct. 2018.

[6] Y. Chen, Y. S. Zheng, and X. R. Miao, "AC breakdown characteristics of air insulated point-plane gaps with polycarbonate barriers," in *Proceedings of 2016 IEEE International Conference on High Voltage Engineering and Application* (*ICHVE*), Chengdu, China, 2016, pp. 1–4.

[7] A. Kara, O. Kalenderli, and K. Mardikyan, "Modeling and analyzing barrier effect on AC breakdown strength of non-uniform air gaps," *IEEE Transactions on Dielectrics and Electrical Insulation*, vol. 24, no. 6, pp. 3416–3424, Dec. 2017.

[8] Y. Z. Cui, C. J. Zhuang, and R. Zeng. "Electric field measurements under DC corona discharges in ambient air by electric field induced second harmonic generation," *Applied Physics Letters*, vol. 115, no. 24, pp. 244101, Nov. 2019.

[9] Q. Hu, Q. M. Li, Z. P. Liu, N. F. Xue, J. Wang, and M. Haddad, "Surface charge accumulation characteristics on DC GIL three-post insulators considering the influence of temperature gradient," *CSEE Journal of Power and Energy Systems*, vol. 9, no. 5, pp. 1926–1934, Sep. 2023.

[10] S. C. Wu, G. Chen, Y. M. Shao, H. Xu, X. N. Zhang, Y. Y. Liang, and Y. P. Tu, "Charge accumulation characteristics of SF_6-epoxy interface under negative repetitive nanosecond pulses," *CSEE Journal of Power and Energy Systems*, vol. 10, no. 4, pp. 1808–1815, Jul. 2024.

[11] B. X. Du and A. Li, "Effects of DC and pulse voltage combination on surface charge dynamic behaviors of epoxy resin," *IEEE Transactions on Dielectrics and Electrical Insulation*, vol. 24, no. 4, pp. 2025–2033, Jan. 2017.

[12] Y. S. Zheng, Q. Q. Li, Y. Chen, S. W. Shu, and C. J. Zhuang, "Breakdown path and condition of air-insulated rod-plane gap with polymeric barrier inserted under alternating voltages," *AIP Advances*, vol. 9, no. 10, pp. 105207, Sep. 2019.

[13] A. Pedersen and A. Blaszczyk, "An engineering approach to computational prediction of breakdown in air with surface charging effects," *IEEE Transactions on Dielectrics and Electrical Insulation*, vol. 24, no. 5, pp. 2775–2783, Oct. 2017.

[14] S. Akram, J. Castellon, and S. Agnel, "Progress in gas/solid interface charging phenomena," *Coatings*, vol. 10, no. 12, pp. 1184, Dec. 2020.

[15] W. K. Pan, Y. Wang, H. Ding, E. Z. Shen, Z. S. Zhang, X. Yang, Z. Z. Wang, and S. Akram, "Nonlinear materials applied in HVDC gas insulated equipment: from fundamentals to applications," *IEEE Transactions on Dielectrics and Electrical Insulation*, vol. 28, no. 5, pp. 1588–1603, Oct. 2021.

[16] Y. Z. Cui, C. J. Zhuang, X. Zhou, and R. Zeng, "The dynamic expansion of leader discharge channels under positive voltage impulse with different rise times in long air gap: experimental observation and simulation results," *Journal of Applied Physics*, vol. 125, no. 11, pp. 113302, Feb. 2019.

[17] X. Li, W. D. Liu, Y. Xu, W. J. Chen, and J. G. Bi, "Surface charge accumulation and pre-flashover characteristics induced by metal particles on the insulator surfaces of 1100 kV GILs under AC voltage," *High Voltage*, vol. 5, no. 2, pp. 134–142, Apr. 2020.

[18] B. X. Du, W. B. Zhu, J. Li, Y. Q. Xing, and P. H. Huang, "Temperature-dependent surface charge behavior of polypropylene film under DC and pulse voltages," *IEEE Transactions on Dielectrics and Electrical Insulation*, vol. 24, no. 2, pp. 774–783, Apr. 2017.

[19] D. Y. Li, G. X. Zhang, T. Y. Wang, and Y. C. Hou, "Charge accumulation characteristic on polymer insulator surface under AC voltage in air and C_4F_7N/CO_2 mixtures," *High Voltage*, vol. 5, no. 2, pp. 160–165, Apr. 2020.

[20] H. K. Meyer, F. Mauseth, R. Marskar, A. Pedersen, and A. Blaszczyk, "Streamer and surface charge dynamics in non-uniform air gaps with a dielectric barrier," *IEEE Transactions on Dielectrics and Electrical Insulation*, vol. 26, no. 4, pp. 1163–1171, Aug. 2019.

[21] Y. L. Wang, Q. Q. Li, S. W. Shu, and Y. S. Zheng, "Residual charges on barrier surface revealed by potential distribution in a hybrid gas-solid insulation system," in *Proceedings of 2020 IEEE International Conference on High Voltage Engineering and Application* (*ICHVE*), Beijing, China, 2020, pp. 1–4.

[22] Y. Du, Y. P. Meng, K. Wu, X. Z. Ma, W. J. Song, and X. Yang, "Influence of gas flow on surface charge decay of partial discharge under DC voltage," in *Proceedings of the 12th International Conference on the Properties and Applications of Dielectric Materials* (*ICPADM*), Xi'an, China, 2018, pp. 132–135.

[23] M. Q. Yuan, L. Zou, Z. Z. Li, L. Pang, T. Zhao, L. Zhang, J. R. Zhou, P. Xiao, S. Akram, and Z. Z. Wang, "A review on factors that affect surface charge accumulation and charge-induced surface flashover," *Nanotechnology*, vol. 32, no. 26, pp. 262001, Arp. 2021.

[24] Y. Gao, N. Li, J. Li, B. X. Du, and Z. Y. Liu, "Charge transport behavior in gamma-ray irradiated poly(ethylene terephthalate) estimated by surface potential decay," *High Voltage*, vol. 6, no. 3, pp. 435–447, Jun. 2021.

[25] S. T. Li, "Improvement of surface flashover in vacuum," *High Voltage*, vol. 5, no. 2, pp. 122–133, Apr. 2020.

[26] B. X. Du, Z. R. Yang, Z. L. Li, and J. Li, "Surface charge behavior of silicone rubber/SiC composites with field-dependent conductivity," *IEEE Transactions on Dielectrics and Electrical Insulation*, vol. 24, no. 3, pp. 1340–1348, Jun. 2017.

[27] S. Akram, K. Zhou, P. F. Meng, J. Castellon, S. Agnel, P. Wang, M. T. Nazir, Y. D. Chen, and H. Hussain, "Charge transport and trapping of surface modified stator coil insulation of motors," *IEEE Transactions on Dielectrics and Electrical Insulation*, vol. 28, no. 2, pp. 719–726, Apr. 2021.

[28] A. Fatihou, L. Dascalescu, N. Zouzou, M. B. Neagoe, A. Reguig, and L. M. Dumitran, "Measurement of surface potential of non-uniformly charged insulating materials using a non-contact electrostatic voltmeter," *IEEE Transactions on Dielectrics and Electrical Insulation*, vol. 23, no. 4, pp. 2377–2384, Aug. 2016.

[29] B. X. Du, J. N. Dong, J. Li, H. C. Liang, and X. X. Kong, "Gas convection affecting surface charge and electric field distribution around tri-post insulators in $\pm$800 kV GIL," *IEEE Transactions on Dielectrics and Electrical Insulation*, vol. 28, no. 4, pp. 1372–1379, Aug. 2021.

[30] Y. Gao, J. L. Wang, F. Liu, and B. X. Du, "Surface potential decay of negative corona charged epoxy/Al_2O_3 nanocomposites degraded by 7.5-MeV electron beam," *IEEE Transactions on Plasma Science*, vol. 46, no. 7, pp. 2721–2729, Jul. 2018.

[31] S. Akram, M. S. Bhutta, K. Zhou, P. F. Meng, J. Castellon, P. Wang, G. Rasool, M. Aamir, and M. T. Nazir, "DC breakdown of XLPE modulated by space charge and temperature dependent carrier mobility," *IEEE Transactions on Dielectrics and Electrical Insulation*, vol. 28, no. 5, pp. 1514–1522, Oct. 2021.

[32] F. B. Meng, X. R. Chen, C. Dai, M. T. Zhang, A. Paramane, L. Zheng, and Y. Tanaka, "Effect of thermal ageing on physico-chemical and electrical properties of EHVDC XLPE cable insulation," *IEEE Transactions on Dielectrics and Electrical Insulation*, vol. 28, no. 3, pp. 1012–1019, Jun. 2021.

[33] F. S. Zhou, J. Y. Li, Z. M. Yan, X. Zhang, Y. Q. Yang, L. M. Jia, D. M. Min, and S. T. Li, "Investigation of charge trapping and detrapping dynamics in LDPE, HDPE and XLPE," *IEEE Transactions on Dielectrics and Electrical Insulation*, vol. 23, no. 6, pp. 3742–3751, Dec. 2016.

[34] A. T. Hoang, Y. V. Serdyuk, and S. M. Gubanski, "Charge transport in LDPE nanocomposites part II—computational approach," *Polymers*, vol. 8, no. 4, pp. 103, Mar. 2016.

[35] Y. P. Meng, W. J. Song, Y. Du, K. Wu, and J. Wu, "Investigation of surface charge distribution on different polymer materials under AC voltage," in *Proceedings of 2016 International Conference on Condition Monitoring and Diagnosis* (*CMD*), Xi'an, China, 2016, pp. 972–975.

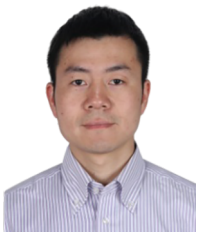

Yuesheng Zheng received the B.Sc. degree in Thermal Energy and Power Engineering from Xi'an University of Technology, Xi'an, China, in 2004, the M.Sc. degree in Electrical Engineering from Xi'an Jiaotong University, Xi'an, China, in 2007, and the Ph.D. degree in Electrical Engineering from Tsinghua University, Beijing, China, in 2012. From 2012 to 2013, he was a postdoctoral researcher at the Chalmers University of Technology, Gothenburg, Sweden. He became the Qishan Scholar in College of Electrical Engineering and Automation, Fuzhou University, Fuzhou, China, in 2014. He has been a Professor at Fuzhou University since 2016. His research interests include gas-solid hybrid insulation, high voltage testing technology, and numerical simulation of electromagnetic fields.

Qinfeng Liao is pursuing an M.S. degree in Fuzhou University. His main research interest is high voltage and new insulation technology.

Bing Deng received the B.Eng. and M.Eng. degrees from Fuzhou University in 2015 and 2018, respectively. His research interest is high voltage and new insulation technology.

Yilong Wang received the B.E. degree in Electrical Engineering from Fuzhou University, Fuzhou, China, in 2018. He is currently pursuing the Ph.D. degree in the College of Electrical Engineering and Automation in Fuzhou University. His main research interest is gas discharge.

Yuriy Serdyuk received the M.Sc. (high voltage engineering) and Ph.D. (high voltage engineering) degrees from the National Technical University of Ukraine, "Kiev Polytechnic Institute" Kiev, Ukraine, in 1986 and 1995, respectively. From 1986, he worked at the Institute of Electrodynamics of the National Academy of Science of Ukraine, Kiev. Since 1999, he is with Chalmers University of Technology, Gothenburg, Sweden, where he is currently a Professor in High Voltage Engineering. His research interests include charge transport and associated processes in dielectric materials for high-voltage applications, and computer simulations of electromagnetic and thermal phenomena in components of power systems.